Available online at www.sciencedirect.com
ScienceDirect
Applied Catalysis B: Environmental 78 (2008) 61–72
APPLIED CATALYSIS B: ENVIRONMENTAL
www.elsevier.com/locate/apcatb

Simultaneous removal of NO_x and diesel soot over nanometer Ln-Na-Cu-O perovskite-like complex oxide catalysts

Jian Liu, Zhen Zhao *, Chun-ming Xu, Ai-jun Duan

State Key Laboratory of Heavy Oil Processing, China University of Petroleum, Beijing 102249, China

Received 20 January 2006; received in revised form 28 August 2007; accepted 3 September 2007
Available online 7 September 2007

Abstract

The nanometric Ln-Na-Cu-O (Ln = La, Pr, Nd, Sm, Gd) perovskite-like complex oxide catalysts were prepared by sol–gel auto-combustion method using citric acid as a ligand and an adjusting agent of particle-size and morphology. Their structures and physico-chemical properties were examined by chemical analysis, XRD, SEM, FT-IR, H_2-TPR and MS-NO-TPD. The catalytic performances of these perovskite-like oxides for the simultaneous removal of soot and NO_x were investigated by a technique of the temperature-programmed reaction (TPR). In the Ln-Na-Cu-O catalysts, the partial substitution of Na for La at A-site led to the formation of Cu^{3+} and/or oxygen vacancy, thus the catalytic activity was remarkably enhanced. The optimal substitution amount of Na (x) is equal to 0.3 for the reduction of NO_x, and x is equal to 0.7 for soot combustion. Moreover, attributing to the effects of very small surface particle sizes of the catalysts and the strong oxidizing ability of NO_2 which was produced from NO and O_2 in the reactant gases on these catalysts, the nanometric Ln-Na-Cu-O perovskite-like oxides exhibit very high catalytic activities for soot combustion even under loose contact conditions between soot and the catalyst.

Keywords: Nanometer; Ln-Na-Cu-O perovskite-like complex oxides; Soot; NO_x; Simultaneous removal

1. Introduction

Diesel-powered vehicles, because of their high thermal efficiency, emit less CO and unburned hydrocarbons than gasoline-fueled vehicles, but the emission of soot particulates and NO_x are still high. Since the reduction of both soot and NO_x emissions to the regulated level cannot be accomplished by engine modifications alone, after-treatment techniques for the simultaneous reduction of their emissions from diesel exhaust should be developed [1–3]. As one possible process, Yoshida et al. proposed the simultaneously catalytic conversion of soot and NO_x into CO_2 and N_2 in an oxidizing atmosphere by using catalyzed soot traps [4]. Although this method involves many technological difficulties to be overcome (the development of efficient and thermally stable traps, the contact between catalyst and trapped soot, etc.), the active catalysts are considered to be the most important one [5].

For the simultaneously removal of soot and NO_x reaction, Teraoka et al. and other researches have done many explorative and pioneering works using perovskite and spinel oxides [5–12]. In addition, the substitutional incorporation of alkali metal into A-sites of perovskite-type (ABO_3) oxides was quite effective in enhancing the activity and selectivity for the NO_x-O_2-soot reaction [8–10]. Teraoka et al. found that La-K-Mn-O perovskite-type oxides were good candidate catalysts for diesel soot combustion [11], and Fino et al. reported that $La_{2-x}K_xCu_{1-y}V_yO_4$ layered oxides had good catalytic performances for the combined removal of diesel particulates and NO_x [9], but they reported the relevant catalytic activities under tight contact conditions between catalysts and soot particles. However, it is a loose contact between the catalysts on the surface of filter and soot particles under practical conditions [13,14]. Thus, it is rather significant to study and design the active catalysts for soot particulate oxidation under loose contact conditions. In recent years, Oi-Uchisawa et al. reported that a platinum catalyst oxidized NO to NO_2, which subsequently oxidized soot to CO and CO_2. So, NO_2 is used as intermediate to facilitate an

* Corresponding author at: Faculty of Chemical Science and Engineering, State Key Lab of Heavy Oil Processing, China University of Petroleum, Beijing, 18#, Fuxue Road, Chang Ping District, Beijing 102249, China.
Tel.: +86 10 89731586.
E-mail address: zhenzhao@cup.edu.cn (Z. Zhao).

0926-3373/$ – see front matter © 2007 Elsevier B.V. All rights reserved.
doi:10.1016/j.apcatb.2007.09.001

indirect contact between the platinum catalyst and soot. The catalyst system is the best one so far reported for soot combustion under loose contact conditions [15,16]. The high oxidation rate of soot is due to the strong oxidizing ability of NO_2. In the present study, we found that a similar mechanism existed on the $La_{2-x}Na_xCuO_4$ perovskite-like complex oxide catalysts, i.e., NO_2 indirectly catalyzed soot combustion. Therefore, this series of catalysts hold good catalytic activities for soot combustion under loose contact conditions between soot and the catalysts.

Catalytic materials exist in various forms and their preparation involves different protocols with a multitude of possible preparation schemes. Moreover, preparation of any catalyst involves a sequence of several complex processes, and many of them are not completely understood. As a result, subtle changes in the preparative details may result in dramatic alteration of the final catalyst properties. Applications of catalyst materials depend on their sizes and morphology. Therefore, much emphasis has been laid on the shape control and the size control recently [17,18]. The surface particle sizes of nanometer material are small. Surface atoms on nanometer catalysts have extra and high surface energies and they are good at mobility, therefore the contact is still very good between catalysts and soot even under loose contact conditions. The development of adequate synthetic methods for the preparation of nanometric powders at low temperatures and atmospheric pressure is a task of great interest. The preparation of such materials may vary in different methods and conditions. Sol–gel technique is one of the most efficient methods, since it permits a better control of stoichiometry, high reactivity, controlled dimensions and nanoparticles. Auto-combustion is a novel way and a unique combination of the combustion process and the chemical gelation process. The process exploits the advantages of cheap precursors, a simple preparation method, and a resulted ultrafine, homogeneous, highly reactive powder [18,19]. In this study, the nanometer Ln-Na-Cu-O perovskite-like complex oxides were prepared by the sol–gel auto-combustion method using additive agent of citric acid. The substitution amounts of A-site cation affect on the catalyst structure and catalytic performances for the simultaneous removal of NO_x and soot under loose contact conditions. The probable reasons which can lead to the activity enhancement for the Na substitution samples compared to the unsubstitution sample were discussed.

2. Experimental

2.1. Catalyst preparation

Two series of Ln_2CuO_4 (Ln = La, Pr, Nd, Sm, Gd) and $La_{2-x}Na_xCuO_4$ ($x = 0$, 0.1, 0.3, 0.5, 0.7, 0.9) perovskite-like complex oxides were prepared by the sol–gel auto-combustion method. The nitrates of Ln, Na and Cu were used as starting materials for obtaining an aqueous solution of Ln^{3+}, Na^+ and Cu^{2+} with appropriate stoichiometry. A solution of citric acid 100% in excess was chosen as a ligand and an adjusting agent of particle-size and morphology. The resulting solution was heated by constant stirring at temperatures of 80–90 °C. After about 50% of water evaporated, the solution was placed in the static air at 90 °C. The clear solution gradually turned milky sol and finally transformed into gel. The gel was translucent with a honey-like color and viscosity. Then, the wet gel was dried homogenously in a stream of air at 120 °C for 4 h. The resulting loosened and foamy solid auto burnt or exploded by heating with an electric furnace. Finally, the precursor was calcinated at 800 °C for 4 h in static air. This technique is particularly suitable to producing nanometric particle samples. For comparison, the two catalysts among the above samples, i.e., $La_{1.7}Na_{0.3}CuO_4$ and $La_{1.3}Na_{0.7}CuO_4$ were further treated. They were compressed at 10 MPa, followed by grinding and sieving at 40–80 meshes. Then, the two samples were calcinated at 900 °C for 10 h in static air. As a result, two non-nanometric catalysts were also prepared, and they were named as La7-9 and La3-9, respectively.

2.2. Catalyst characterization

The crystal structures of the fresh catalysts were determined by a powder X-ray diffractometer (Shimadzu XRD 6000), using Cu Kα (λ = 1.54184 Å) radiation combined with Nickel filter operating at 40 kV and 10 mA. The diffractometer data were recorded for 2θ values between 15° and 80° with a scanning rate of 4°/min. The patterns were compared with JCPDS reference data for phase identification. The Scherrer equation was used to calculate the crystal size of the studied samples. The morphology of the catalysts was observed by SEM (S-4300, Japan).

FT-IR absorbance spectra were obtained in the wave number ranging between 6000 and 400 cm^{-1} via a FTS-3000 spectrophotometer manufactured by American Digilab company. The measured wafer was prepared as KBr pellet with the weight ratio of sample to KBr, 1/100. The resolution was set at 2 cm^{-1} during measurements.

H_2-TPR measurements were performed in a conventional flow apparatus. Two hundred milligrams sample was pretreated in an air atmosphere by calcination at 600 °C for 1 h and subsequently cooled to 100 °C with helium flowing. Afterwards, the H_2-TPR was carried out using 10% hydrogen in helium at constant flow rate of 30 cm^3/min, from 100 to 900 °C, at a heating rate of 10 °C/min. The hydrogen consumption signal was monitored by a thermal conductivity detector (TCD) in an on-line gas chromatograph (GC). For eliminating the effect of the outlet reactor gas containing other components which mainly consisted of H_2O and CO_2 on the TCD for H_2-TPR measurements, it was set a filter that contained 5A molecular sieve (60–80 meshes) for adsorption of H_2O and CO_2 before the reaction gases entering the TCD.

MS-NO-TPD detected by mass spectrometry was carried out on Quantachrome autosorb-1C mass spectroscope. The samples were first heated from room temperature to 800 °C at a rate of 20 °C/min and kept at 800 °C for 1 h in helium. The pretreated sample was first cooled to 200 °C at the same atmosphere, then swept with 4000 ppm NO (helium balanced) for the adsorption of NO for 1 h, and cooled to 100 °C in the NO stream for 0.5 h again. Hereafter, swept with helium at a rate of

30 ml/min until the base line of the signal became flat and steady. Finally, the sample was heated at a rate of 20 °C/min in helium to record the TPD spectra.

2.3. Activity measurement

The catalytic activities of the prepared samples were evaluated with a TPR reaction on a fixed-bed tubular quartz system. The reaction temperature was controlled through a PID-regulation system based on the measurements of a K-type thermocouple and varied during each TPR run from 200 to 700 °C at a 2 °C/min rate. The soot used in this work was Printex-U which was supplied by Degussa as a model soot. Its primary particle size was 25 nm and specific surface area was 100 m^2/g. The catalyst and soot were mixed with a spatula in order to reproduce the loose contact mode, which is the most representative model of diesel particles flowing through a catalytic filter [13]. One hundred and eighty milligrams of the mixture (catalyst to soot, 5:1, w/w) was placed in the tubular quartz reactor (ϕ = 10 mm) in every testing. Reactant gases containing 5% O_2 and 0.2% NO balanced with He were passed through a mixture of the catalyst and soot at a flow rate of 50 ml/min. The outlet gas from the reactor passed through a 1 cm^3 sampling loop of a six-point gas-sampling valve before it was being injected into an on-line GC. The GC used both a thermal conductivity detector and a flame ionization detector (FID) to analyze the gaseous mixture composition. The TCD was used to measure the concentration of O_2, N_2, CO and NO after separating these gases over molecular sieve 5A column. The FID was employed to determine CO and CO_2 concentrations after separating these gases over a Porapak N column and converting them to methane over a Ni catalyst at 380 °C.

Further TPR experiments over two typical catalysts ($La_{1.7}Na_{0.3}CuO_4$ and $La_{1.3}Na_{0.7}CuO_4$) were carried out by mass spectrometer (MS) detector using different reactant gas compositions:

(1) 5% O_2 and 0.2% NO balanced with He;
(2) 5% O_2 and 0.2% NO balanced with He, 5% O_2 with He, or 0.2% NO balanced with He.

It was difficult to distinguish two species with the same mass number such as CO and N_2 if only the first strong signal line was used during mass spectroscopy detection. Thus, the second strong signal line was applied to help to check the concentrations of CO, N_2 and CO_2, N_2O in order to distinguish two species with the same mass number. During the measurement the mass numbers of 12, 28, 44 and 14 were used for CO, N_2, CO_2 and N_2O, respectively. The concentration of N_2O has also excluded the influence of NO and N_2. In addition, the catalytic activity results of GC detection were applied to verify the concentrations of these species at peak value.

Another group of explorative experiments were performed on the above fixed beds for studying on the NO adsorption under the oxygen-rich conditions. Reactant gas compositions were 5% O_2 and 0.2% NO with He balanced gas. The reaction temperature ranged from 200 to 600 °C. The catalyst used was 200 mg and without soot during the reaction. The other reaction conditions were the same as ones mentioned above TPR experiment. The composition analyzing of outlet gas was also performed on the mass spectrometer detector.

3. Results

3.1. Catalyst characterization

3.1.1. Defective structure of $La_{2-x}Na_xCuO_4$

The differences of A-site atoms in perovskite-like mixed oxides may lead to the differences of their physcio-chemical properties. For different rare earth ions at A-site, the differences of their physico-chemical properties are not obvious in Ln_2CuO_4. Some Cu^+ and oxygen vacancy (V_o) formed in the Ln_2CuO_4 oxides (Ln = Pr, Nd, Sm, Gd). However, in the series of $La_{2-x}Na_xCuO_4$ oxides, the deficient positive charge resulting from the substitution of Na^+ for La^{3+} could be balanced either by the formation of higher oxidation state ions at B-site, i.e., $Cu^{2+} \rightarrow Cu^{3+}$, or by the formation of oxygen vacancy. In fact, the two cases often occur at the same time. The average valence of Cu ions and the contents of Cu^{3+} (Cu^+) or Cu^{2+} in the two series of oxides were determined by the chemical analysis using the method of iodometry [20]. The oxygen nonstoichiometry (λ) was calculated [21]. The variation of the average valence of Cu ions, λ and the Cu ion contents are also shown in Table 1. The analysis results show that the contents of Cu^+ or Cu^{2+} and λ had similar values in the different Ln_2CuO_4 samples, while there was a remarkable change of the contents of Cu^{3+} or Cu^{2+}

Table 1
The average valence of Cu ions, nonstoichiometric oxygen (λ) and the Cu ion content in the Ln_2CuO_4 and $La_{2-x}Na_xCuO_4$ systems (wt%) (Ln = La, Pr, Nd, Sm, Gd, and x = 0, 0.1, 0.3, 0.5, 0.7, 0.9)

Catalysts	Cu^{2+} (wt%)	Cu^+ (wt%)	Cu^+/Cu^{2+}	Cu^{3+} (wt%)	Cu^{3+}/Cu^{2+}	Average valence of Cu	λ
La_2CuO_4	0.1551	–	–	0.0003	0.0019	2.0019	0.0002
Pr_2CuO_4	0.1624	0.0051	0.0313	–	–	1.9677	−0.0040
Nd_2CuO_4	0.1564	0.0026	0.0165	–	–	1.9832	−0.0021
Sm_2CuO_4	0.1524	0.0071	0.0468	–	–	1.9509	−0.0061
Gd_2CuO_4	0.1510	0.0068	0.0450	–	–	1.9528	−0.0059
$La_{1.9}Na_{0.1}CuO_4$	0.1544	–	–	0.0064	0.0414	2.0397	−0.0200
$La_{1.7}Na_{0.3}CuO_4$	0.1556	–	–	0.0160	0.1031	2.0934	−0.0633
$La_{1.5}Na_{0.5}CuO_4$	0.1809	–	–	0.0121	0.0670	2.0628	−0.1171
$La_{1.3}Na_{0.7}CuO_4$	0.1828	–	–	0.0124	0.0677	2.0634	−0.1671
$La_{1.1}Na_{0.9}CuO_4$	0.1751	–	–	0.0116	0.0661	2.0620	−0.1572

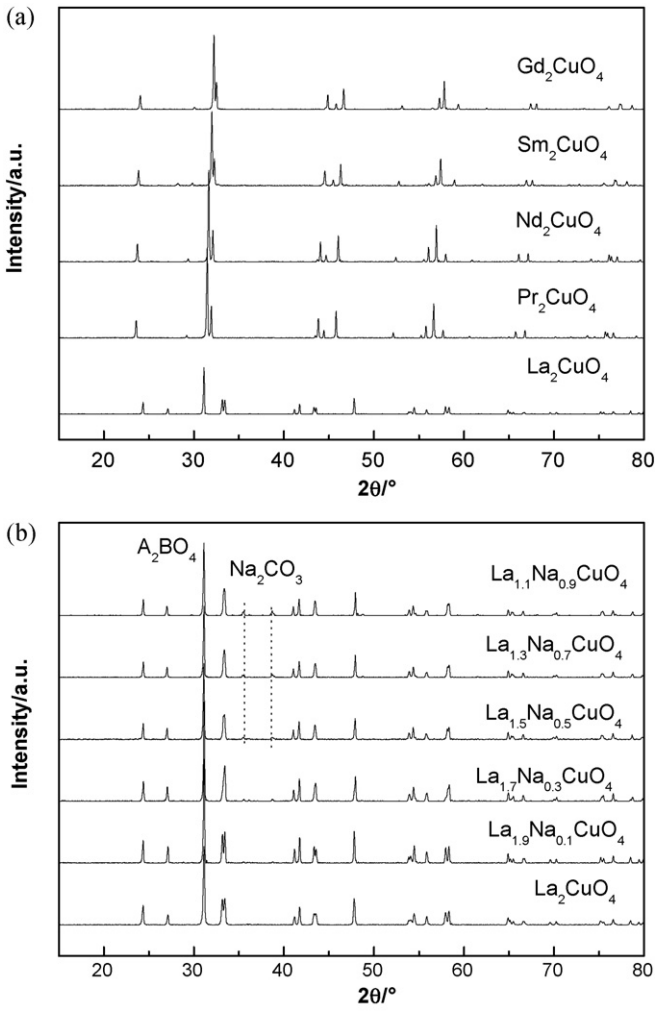

Fig. 1. X-ray diffraction patterns of Ln_2CuO_4 and $La_{2-x}Na_xCuO_4$ catalysts. (a) Ln_2CuO_4 (Ln = La, Pr, Nd, Sm, Gd) and (b) $La_{2-x}Na_xCuO_4$ ($x = 0, 0.1, 0.3, 0.5, 0.7, 0.9$).

and λ in the $La_{2-x}Na_xCuO_4$ system. In the range of $0.0 \leq x \leq 0.3$, the contents of Cu^{3+} increased rapidly with λ and thus, the charge of the mixed oxides were mainly balanced by the increase of Cu^{3+}. On the other hand, in the range of $0.5 \leq x \leq 0.9$, the formation of oxygen vacancies was more pronounced. Cu^{3+} amount was the largest in $La_{1.7}Na_{0.3}CuO_4$, however, $La_{1.3}Na_{0.7}CuO_4$ had the maximal concentration of oxygen vacancies.

3.1.2. The results of XRD

In perovskite-like mixed oxides (A_2BO_4), when A atoms are different rare earth elements, such as La, Pr, Nd, Sm, and Gd, their crystal structures change to some extent. Fig. 1a shows that La_2CuO_4 has orthorhombic (O) K_2NiF_4 phase, and Ln_2CuO_4 (Ln = Pr, Nd, Sm, Gd) samples have T′ phase. In octahedron of La_2CuO_4, Cu has six coordination O atoms, in which the bond length of Cu–O is longer than those in Ln_2CuO_4 (Ln = Pr, Nd, Sm, Gd), whose Cu atom has four coordinated O atoms [22]. For the $La_{2-x}Na_xCuO_4$ catalysts, as shown in Fig. 1b, the XRD patterns gave several large peaks at 31.1°, 47.8° and 33.4°. It reveals that the complex oxides of $La_{2-x}Na_xCuO_4$ possessed A_2BO_4 perovskite-like structures [21,22]. When the Na-substitution amount was small, for example, the $La_{1.9}Na_{0.1}CuO_4$ possessed orthorhombic K_2NiF_4 structure. However, the structural symmetry of $La_{2-x}Na_xCuO_4$ enhanced when $x \geq 0.3$, i.e., the structures of $La_{2-x}Na_xCuO_4$ changed into tetrahedral K_2NiF_4 structures from octahedral ones. This conclusion was supported by the changing from two diffraction peaks to one peak at around 33° and 54°. Moreover, when Na substitution amount was equal to or exceeds 0.5, there existed a trace amount of Na_2CO_3.

Table 2 shows that the average crystal particle sizes of Ln_2CuO_4 and $La_{2-x}Na_xCuO_4$ samples are between 44 and 58 nm. Furthermore, as shown in Fig. 2, SEM photographs of La_2CuO_4, $La_{1.7}Na_{0.3}CuO_4$ and $La_{1.3}Na_{0.7}CuO_4$ exhibit that the catalyst particles had an average particle size centered around 60 nm with a spherical shape. These results reveal that the catalysts which were prepared by the sol–gel auto-combustion method possessed nanometer particle sizes. Moreover, Fig. 2d and e show that the average particle sizes of La7-9 and La3-9 catalysts were larger than 500 nm. It indicates that their particle sizes have exceeded the nanometric range after the $La_{1.7}Na_{0.3}CuO_4$ and $La_{1.3}Na_{0.7}CuO_4$ samples were compressed at high pressure and calcinated at high temperature.

3.1.3. The results of IR

IR spectroscopic results support the above structure analysis by XRD. Fig. 3 depicts the observed IR spectra of these complex oxides. All samples had the vibrational absorption band at around 520 cm^{-1}, which could be attributed to the characteristic absorption band of K_2NiF_4-type structure as well. According to reference, the absorption band around 520 cm^{-1} is attributed to the stretching vibration of A–O–B (i.e., bond

Table 2
The average crystal sizes of Ln_2CuO_4 and $La_{2-x}Na_xCuO_4$ catalysts (Ln = La, Pr, Nd, Sm, Gd, and $x = 0, 0.1, 0.3, 0.5, 0.7, 0.9$)

Catalysts	Crystal face	λ (nm)	I/I1	2θ (°)	β (rad)	D (nm)	$(\varepsilon^2)^{1/2} \times 10^{-3}$
La_2CuO_4	220	0.1542	100	31.1184	0.1860	43.88	2.3256
Pr_2CuO_4	210	0.1542	100	31.4746	0.1436	56.88	1.7741
Nd_2CuO_4	210	0.1542	100	31.6514	0.1388	58.88	1.7048
Sm_2CuO_4	210	0.1542	100	31.9882	0.1555	52.60	1.8887
Gd_2CuO_4	210	0.1542	100	32.2311	0.1593	51.37	1.9195
$La_{1.9}Na_{0.1}CuO_4$	220	0.1542	100	31.1221	0.1448	56.36	1.8103
$La_{1.7}Na_{0.3}CuO_4$	220	0.1542	100	31.1271	0.1414	57.72	1.7675
$La_{1.5}Na_{0.5}CuO_4$	220	0.1542	100	31.0970	0.1455	56.09	1.8206
$La_{1.3}Na_{0.7}CuO_4$	220	0.1542	100	31.1121	0.1506	54.19	1.8834
$La_{1.1}Na_{0.9}CuO_4$	220	0.1542	100	31.1080	0.1439	56.71	1.7999

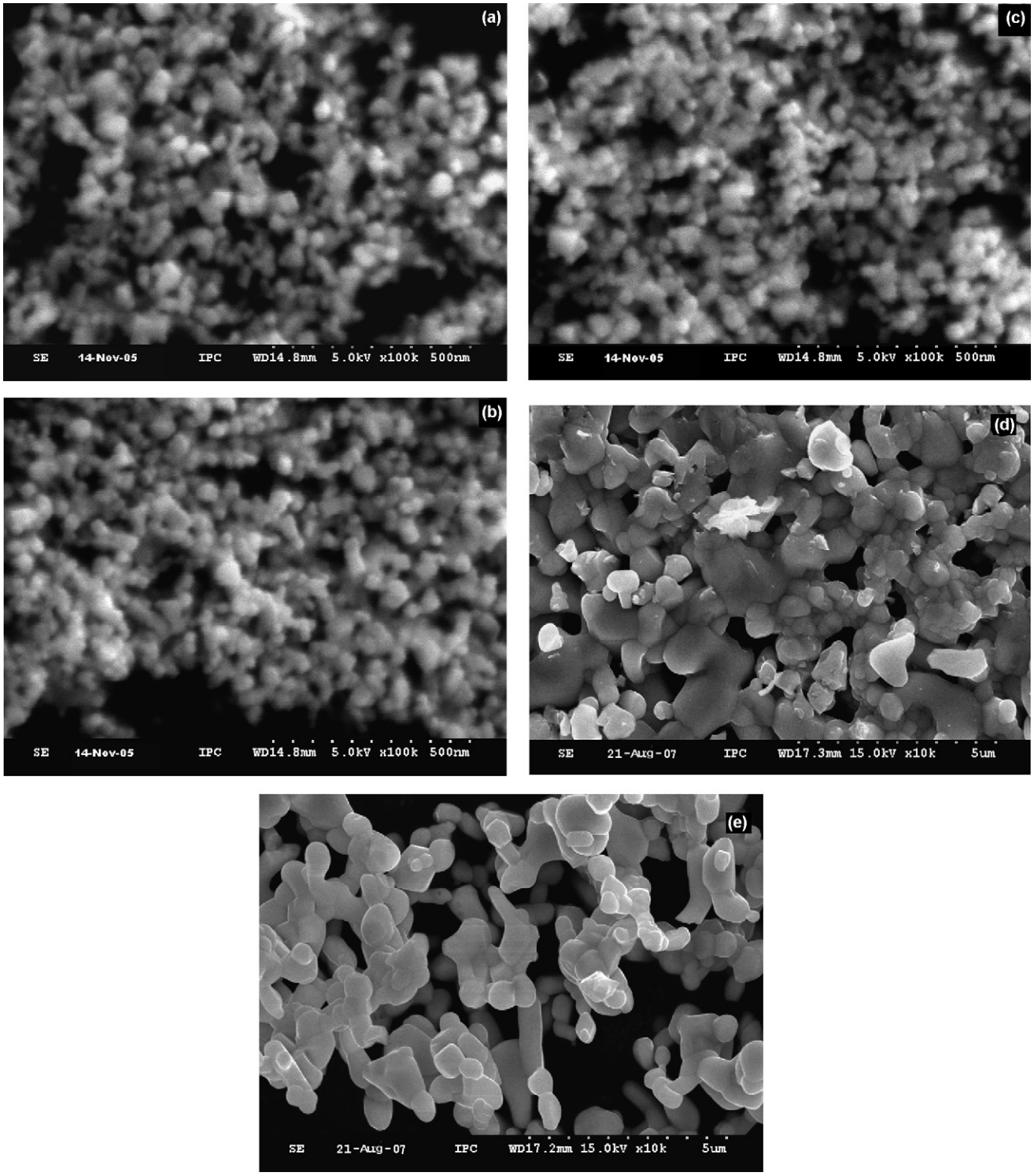

Fig. 2. SEM photographs of several catalysts. (a) La_2CuO_4, (b) $La_{1.7}Na_{0.3}CuO_4$, (c) $La_{1.3}Na_{0.7}CuO_4$, (d) La7-9, and (e) La3-9.

Ln–O–Cu) of A_2BO_4 and it is assigned to the vibration mode of A_{2u} [23]. Fig. 3a shows that La_2CuO_4 had a vibration band around 680 cm^{-1}, but Ln_2CuO_4 (Ln = Pr, Nd, Sm, Gd) had not, which was due to their obvious differences in crystal structures. Meanwhile, Fig. 3a shows that their vibrations around 520 cm^{-1} were also different from each other. With the increase of atomic number (La < Pr < Nd < Sm < Gd), this vibration band shifted to the high wave number except Pr. (The reason of Pr shifting to the lower band may because there are two oxidation states of Pr atom.) The shifting to higher wave number of the band around 550 cm^{-1} demonstrates that A–O and B–O bonds become strong and short. For $La_{2-x}Na_xCuO_4$ catalysts, as shown in Fig. 3b, all of samples had the vibration bands centered at 520 and 690 cm^{-1} in the whole range of $0.0 \leq x \leq 0.9$. The latter is due to the stretching motion of B–O bond of BO_6 octahedra in the direction of *a*- or *b*-axis, and it

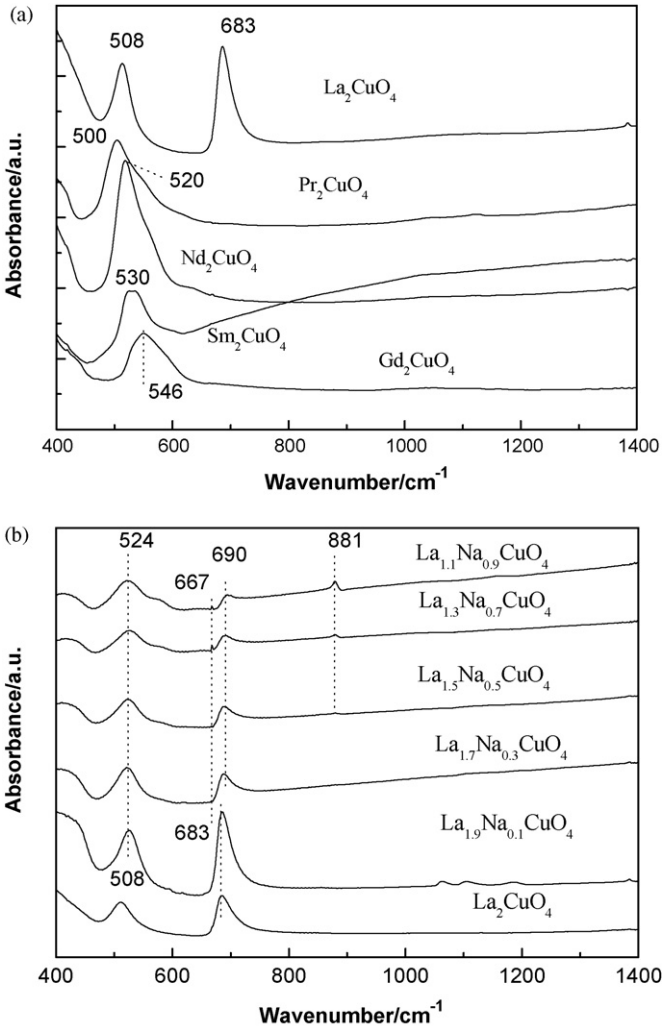

Fig. 3. The FT-IR spectra of Ln_2CuO_4 and $La_{2-x}Na_xCuO_4$ catalysts. (a) Ln_2CuO_4 (Ln = La, Pr, Nd, Sm, Gd) and (b) $La_{2-x}Na_xCuO_4$ (x = 0, 0.1, 0.3, 0.5, 0.7, 0.9).

belongs to the E_{2u} vibration mode [23]. Compared with the unsubstituted sample La_2CuO_4, the vibration bands at ~520 and ~690 cm^{-1} of Na^+-substituted samples become weaker, broader and upshifting. The results further indicate that some amounts of Cu^{2+} changed into Cu^{3+}, which were verified by chemical analysis. Moreover, very weak absorption peaks at 881 cm^{-1} appeared in the IR spectra of $La_{2-x}Na_xCuO_4$ samples when Na substitution amount exceeded or was equal to 0.5. This is attributed to Na–O–C vibration in the Na_2CO_3. It is noted that the small sharp peak near 667 cm^{-1} did not belong to the IR absorption band, and the phenomenon occurred due to the small crystalline particles [21,24].

3.1.4. The results of H_2-TPR

Fig. 4 shows the H_2-TPR profiles of the series of $La_{2-x}Na_xCuO_4$ perovskite-like catalysts. During H_2-TPR process, not only were the metallic cations with high valence reduced to ions with low valance or metal atoms by H_2, but also the lattice oxygen ion involved the process due to H_2O formation. Therefore, the reducibility of metallic ion and the mobility of lattice oxygen can also be reflected by H_2-TPR

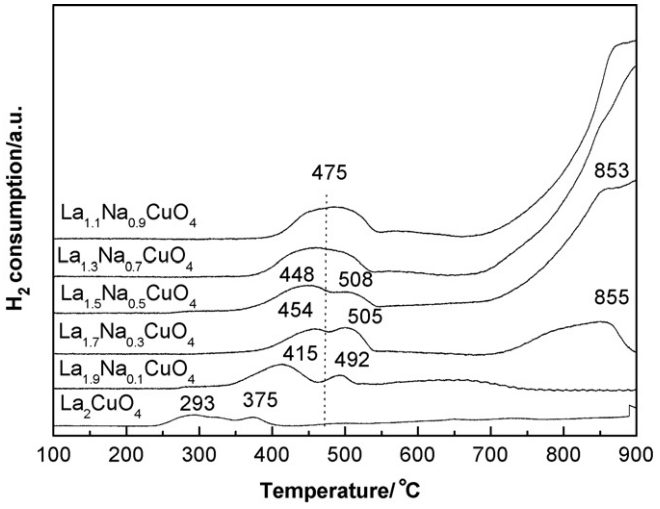

Fig. 4. The H_2-TPR curves of $La_{2-x}Na_xCuO_4$ catalysts (x = 0, 0.1, 0.3, 0.5, 0.7, 0.9).

measurement [25]. There were three kinds of reduction peaks on the H_2-TPR curves of all samples, namely, α (150 °C ≤ T ≤ 450 °C), β (450 °C ≤ T ≤ 700 °C), γ (T ≥ 700 °C). Spinicci and Tofanari demonstrated that the α could be referred to a less negatively charged species O_2^-, β to a more negatively charged species O^- and γ to the lattice oxygen [26]. After the samples were reduced by H_2 at 700 °C, the structure analysis with IR was carried out. The results (not be shown for concision) show that the K_2NiF_4-type structure is still retained after the reduction was carried out till the temperatures corresponding to α and β peaks, which are lower than 700 °C. Owing to a large amount of oxygen vacancies existing in the structure of samples, oxygen will be absorbed after the samples are pretreated in the oxygen atmosphere. So α could be attributed to the following reaction: $Cu^{3+} + O_2^- + 2H_2 \rightarrow Cu^{2+} + 2H_2O$, and β could be ascribed to the following reduction process: $Cu^{3+} + O^- + H_2 \rightarrow Cu^{2+} + H_2O$. As shown in Fig. 5, IR results also reveal that the K_2NiF_4-type structures of the catalysts were destroyed after their reductions were carried out till the

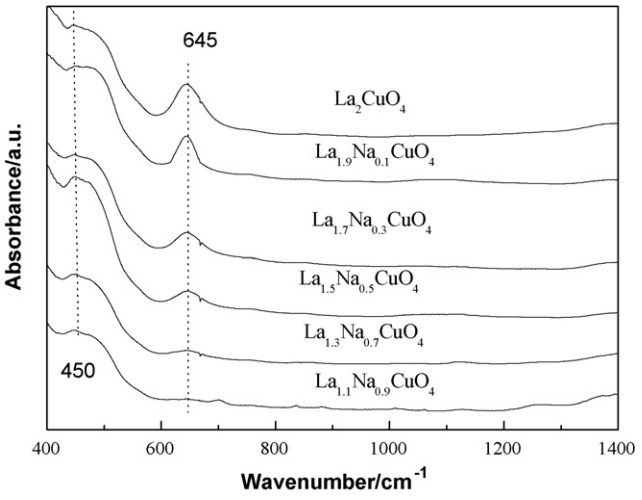

Fig. 5. The FT-IR spectra of $La_{2-x}Na_xCuO_4$ catalysts after H_2-TPR at 900 °C (x = 0, 0.1, 0.3, 0.5, 0.7, 0.9).

Table 3
The reduction peak temperatures and areas of H_2-TPR of $La_{2-x}Na_xCuO_{4-\lambda}$

Catalysts	La_2CuO_4	$La_{1.9}Na_{0.1}CuO_4$	$La_{1.7}Na_{0.3}CuO_4$	$La_{1.5}Na_{0.5}CuO_4$	$La_{1.3}Na_{0.7}CuO_4$	$La_{1.1}Na_{0.9}CuO_4$
T_α (°C)	293, 375	415	454	448	475	475
T_β (°C)	–	492	505	508		
T_γ (°C)	–	–	855	853	>900	>900
S_α (a.u.)	62292	101818	101460	128188	202381	215312
S_β (a.u.)	–	28138	71798	65701		
S_γ (a.u.)	–	–	192549	644703	>875550	>837466

$x = 0, 0.1, 0.3, 0.5, 0.7, 0.9$.

temperature of 900 °C corresponding to γ peak, and the colors of all the samples transformed into red or light red after they were reduced in H_2 atmosphere at 900 °C. It reveals that Cu^{2+} ions were reduced into red Cu_2O (Cu^+) because the metal Cu is not red but black under the condition of high dispersion. In addition, Cu_2O was of high stability in H_2 atmosphere even if at 900 °C. It indicates that γ reduction peak corresponded to the reduction process: $2Cu^{2+} + 2O^{2-} + H_2 \rightarrow Cu_2O + H_2O$. Table 3 shows the reduction peak temperatures and areas of H_2-TPR of $La_{2-x}Na_xCuO_4$ for three stages of reduction in the H_2-TPR process, namely, α, β and γ. According to the temperature ranges of α, β and γ peaks, it seems that O_2^- and O^- should be responsible for the soot combustion. According to the results of Fig. 4 and Table 3, it can be seen that when $x \geq 0.3$ $La_{2-x}Na_xCuO_4$ catalysts not only have the larger areas of α and β peaks, but also their γ peak areas are larger compared to the $La_{2-x}Na_xCuO_4$ samples with small substitution amounts. It indicates that $La_{2-x}Na_xCuO_4$ samples with larger substitution amounts not only have the larger concentration of surface oxygen species (O_2^- and O^-), but also the mobility of their lattice oxygen is stronger. Thus, $La_{2-x}Na_xCuO_4$ samples with larger substitution amounts ($x \geq 0.3$) should have the higher catalytic activities for the title reaction.

3.1.5. The results of MS-NO-TPD

MS-NO-TPD stands for temperature-programmed desorption of NO detected by mass spectrometer. Strictly speaking, MS-NO-TPD should be called accurately as temperature-programmed surface reaction (TPSR), because the adsorbed NO molecules under temperature-programmed desorption (NO-TPD) process may undergo a reaction and turns into other adsorption species such as NO_2, N_2O, N_2 and O_2 and so on. Using this method to study the adsorption and activation of NO molecules over the perovskite-like complex catalysts is significant to reveal the catalysis nature of the NO reduction over these kinds of catalysts. Generally, the adsorption of NO by perovskite and related oxides is related to the surface area and oxygen vacancies under the condition of absent oxygen. The surface area of all these catalysts is small due to calcinations at higher temperature. Therefore, the difference in adsorbed amount of NO on different catalysts would be attributed to the different concentrations of oxygen vacancies. The MS-NO-TPD curves of $La_{2-x}Na_xCuO_4$ are shown in Fig. 6. Table 4 exhibits the reduction peak temperatures and areas of NO or O_2 during NO-MS-TPD over $La_{2-x}Na_xCuO_4$ catalysts. The ratio of (total amount of NO adsorption)/(the amount of oxygen vacancy) is also shown in Table 4. Compared to the nonstoichiometric oxygen contents displayed in Table 1, it reveals that the adsorption amounts of NO by $La_{2-x}Na_xCuO_4$ oxides were related to the oxygen vacancy concentration. From Fig. 6a and Table 4 it can be seen that the relative desorption amounts of NO, i.e., the intensities of NO desorption peak, are closely dependent on the catalyst composition. La_2CuO_4 only had a small NO desorption peak attributing to its small amount of nonstoichiometric oxygen. With the introduction of Na, the intensity of the desorption peak increased. It is due to a large amount of oxygen vacancy formed in the $La_{2-x}Na_xCuO_{4-\lambda}$ samples. Among all of the samples, the peak of NO desorption was the highest over the $La_{1.3}Na_{0.7}CuO_{4-\lambda}$ catalyst below 400 °C, indicating that $La_{1.3}Na_{0.7}CuO_4$ had the maximal concentration of oxygen vacancies. It is consistent with the results of chemical analysis. Fig. 6b shows that the amounts of O_2 desorption increased with the increasing of Na substitution amount. It reveals that the mobility of oxygen in the $La_{2-x}Na_xCuO_4$ samples was enhanced due to the increase of the concentration of oxygen vacancies. Fig. 6c shows that the various gas concentration plots during NO-MS-TPD over a typical $La_{1.3}Na_{0.7}CuO_4$ catalyst. It demonstrates that the adsorbed NO molecules undergo a complex reaction in the NO-TPD process. Furthermore, an explorative study was performed by the reaction gases fed through the fixed bed of any of the prepared $La_{2-x}Na_xCuO_4$ catalyst in the absence of soot. As shown in Fig. 7, the different catalysts absorbed different amounts of NO under the oxygen-rich condition. The amount of absorbed NO was the largest on $La_{1.7}Na_{0.3}CuO_4$ catalyst below 600 °C, which was not fully consistent with the previous MS-NO-TPD results in Fig. 6. It revealed that NO adsorption is also related to other factors besides oxygen vacancy concentration in oxidizing atmosphere, i.e., the presence of oxygen affects the adsorption of NO. It is noted that the peaks of NO change are negative. It is due to that Fig. 7 exhibited NO concentration changes detected by MS in the reaction gas stream. The experimental procedure for the NO absorption on the catalysts was different from that for NO desorption process as shown in Fig. 6. In the process of NO absorption the concentrations of NO were monitored by mass detector in the reaction gas stream. The initial NO concentration was kept at 0.2% in the reaction process. The concentration of NO would decrease when it was adsorbed on catalysts, and it could obtain negative maximum when the absorption rate of NO was the highest. At that time the adsorption of NO reached relative saturation.

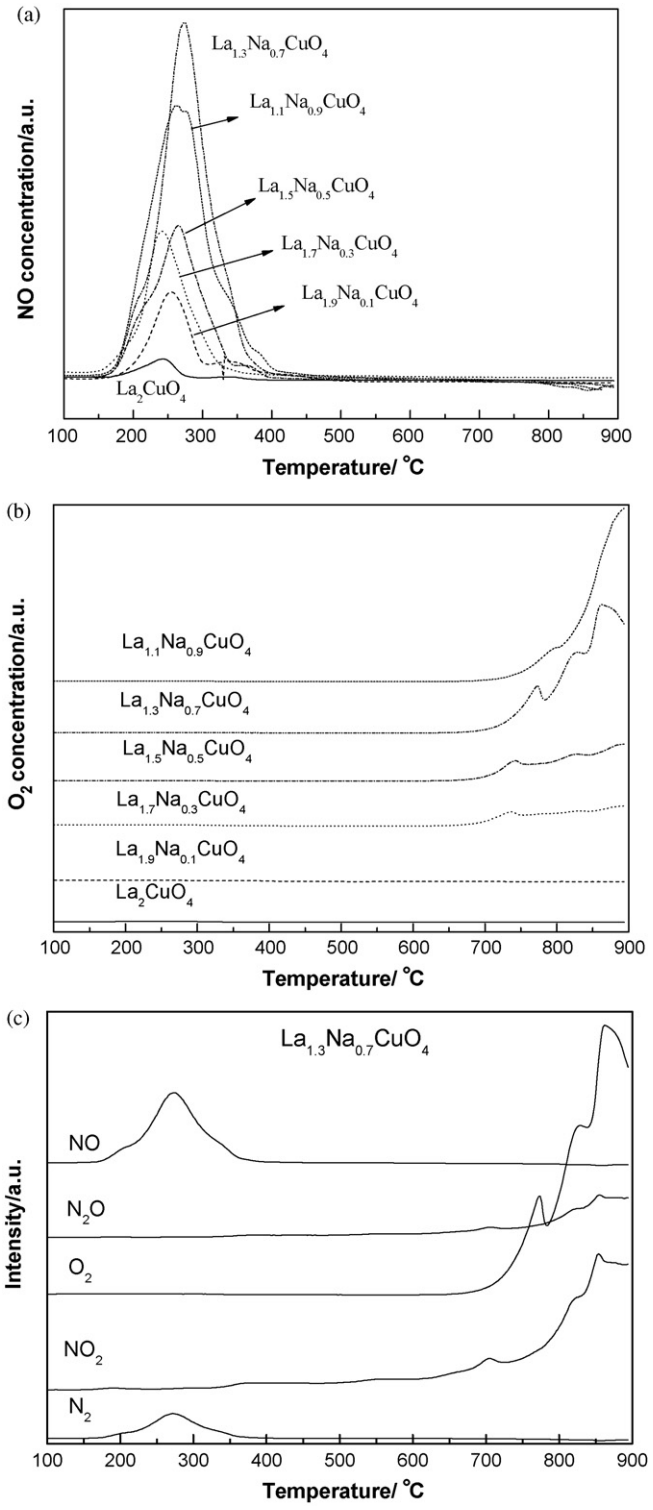

Fig. 6. The outlet NO or O_2 concentration plots for $La_{2-x}Na_xCuO_4$ catalysts or various gas concentration plots for $La_{1.3}Na_{0.7}CuO_4$ catalyst during NO-MS-TPD ($x = 0$, 0.1, 0.3, 0.5, 0.7, 0.9). (a) NO, (b) O_2, and (c) various gas concentration plots.

After that the concentration of NO would go up again attributing to the decreasing of the amount of NO adsorbed or the desorption of NO. Thus, negative peak was obtained for NO concentration changes in Fig. 7.

3.2. The catalytic activity measurement results

The soot conversion was calculated by integration of CO and CO_2 concentrations over the recorded time intervals. The carbon balance was always close to 98%, i.e., not approaching complete conversion, which may ascribe to a little amount soot being oxidized at the low temperature (<200 °C). The selectivity to CO_2 (S_{CO_2}) was defined as that the CO_2 outlet concentration (C_{CO_2}) divided by the sum of the CO_2 and CO outlet concentration, i.e., $S_{CO_2} = C_{CO_2}/(C_{CO} + C_{CO_2})$. The catalytic activity was evaluated by the values of T_{10}, T_{50}, and T_{90}, which were defined as the temperatures by which 10, 50, and 90% of the soot were oxidized during the TPR procedure, respectively. Since in practical applications the rate of carbon oxidation at lower temperatures is more important than the whole of the TPR profile, we especially focus on the results of T_{10} and T_{50}. Another important parameter is P_{N_2}, i.e., the productivity of N_2, $P_{N_2} = 2[N_{2out}]/[NO_{in}]$.

TPR data for the simultaneous removal of NO_x and soot are shown in Table 5. From these data it can be seen that the catalytic activity became gradually lower with the increase of atom number in the system of Ln_2CuO_4 catalysts. However, in the $La_{2-x}Na_xCuO_4$ catalysts, the partial substitution of Na for La at A-site greatly enhanced the catalytic activity for the simultaneous removal of NO_x and diesel soot. The optimal substitution amount of Na (x) was equal to 0.3 for the reduction of NO_x, and x was equal to 0.7 for soot combustion among these samples under loose contact conditions between the catalyst and soot. On the other hand, the temperatures of soot combustion over La7-9 and La3-9 samples were much higher than those of soot oxidation over $La_{1.7}Na_{0.3}CuO_4$ and $La_{1.3}Na_{0.7}CuO_4$ catalysts. It indicates that the particle sizes of catalysts remarkably affected on their catalytic activities for soot combustion.

4. Discussion

4.1. The characteristics of the reaction for the simultaneous removal of NO_x and diesel soot on the Ln-Na-Cu-O catalysts

The soot removal reaction supposedly takes place at the three-phase boundary among a solid catalyst, a solid reactant (soot) and gaseous reactants (O_2, NO). A crucial issue affecting the performance of catalysts for soot combustion lies in the contact conditions between catalyst and soot. The contact between catalytic active sites and the soot, is of great importance for solid–solid reactions [27–29]. Since the number of contact points on the catalysts is proportional to the active site concentration, it even seems that this contact area is a rate-determining factor because the difference in inherent activity of the several species is of less importance than the contact between soot and catalyst, i.e., the concentration of catalytic sites in contact with the soot regardless of their nature. That is because a catalyst will play no role for soot oxidation if the catalyst cannot contact with soot particles. According to the physical property of Printex soot, the primary particle size of

Table 4
The reduction peak temperatures and areas of NO or O_2 during NO-MS-TPD over $La_{2-x}Na_xCuO_4$ catalysts

Catalysts	La_2CuO_4	$La_{1.9}Na_{0.1}CuO_4$	$La_{1.7}Na_{0.3}CuO_4$	$La_{1.5}Na_{0.5}CuO_4$	$La_{1.3}Na_{0.7}CuO_4$	$La_{1.1}Na_{0.9}CuO_4$
T_{NO} (°C)	242	254	242	266	272	260
T_{O_2} (°C)	–	–	740	742	771	890
S_{NO}/E−10	2.45	20.21	47.04	65.78	105.45	102.41
S_{O_2}/E−10	–	–	84.08	116.20	395.82	374.22
S_{NO}/λ (a.u.)	1225	1011	743	562	631	651

x = 0, 0.1, 0.3, 0.5, 0.7, 0.9.

soot is 25 nm. The average pore diameter of modern typical catalysts based on a carrier (e.g. SiO_2) does not exceed 15 nm. Thus, soot particulates cannot enter the inter pores of the catalysts. It is suggested that in the catalytic oxidation of soot only the outer surface of the catalyst plays an important role, as only outer surface can provide the necessary solid–solid contact sites. For supported oxide or noble metal catalysts, their dispersing active species on large specific areas which typically exploited by gaseous reactants are of no use for soot. Therefore, we prepared nanometric powder catalysts in the present study which can provide the best contact conditions between soot and catalysts (e.g. the largest number of contact sites), thus it promoted the catalytic performance for the simultaneous removal of soot and NO_x. The catalytic activity results in Table 5 have exhibited that the temperatures of soot combustion over non-nanometric La7-9 and La3-9 samples were much higher than those of soot oxidation over nanometric $La_{1.7}Na_{0.3}CuO_4$ and $La_{1.3}Na_{0.7}CuO_4$ catalysts. It demonstrates that nanometer effect played an important role in the catalytic combustion of soot.

Fig. 8 shows the typical results of TPR over $La_{1.7}Na_{0.3}CuO_4$ and $La_{1.3}Na_{0.7}CuO_4$ catalysts detected by mass spectrometer. The formation of CO_2 due to oxidation of the soot and the reduction of NO were observed at the similar temperature range. The curves of N_2 and CO_2 formation were very similar in shape. This result suggests the possibility of the simultaneous removal of NO and soot in the perovskite-like samples prepared. The sharp drop of CO_2 formation at temperatures

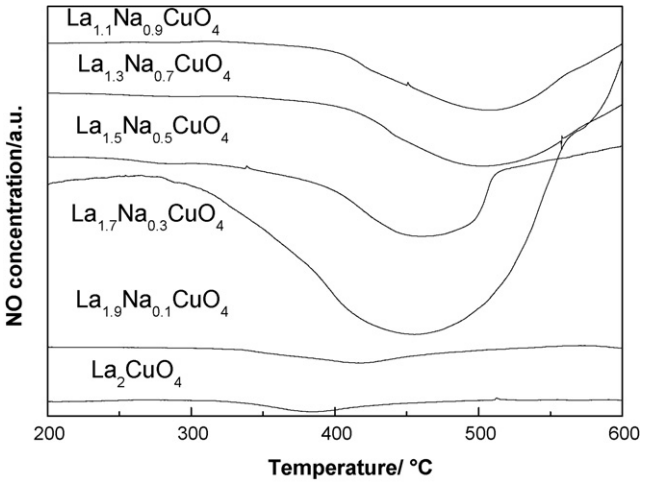

Fig. 7. The outlet NO concentration plots over $La_{2-x}Na_xCuO_4$ catalysts in the absence of soot (x = 0, 0.1, 0.3, 0.5, 0.7, 0.9).

higher than 500 °C is undoubtedly due to the exhaustion of the charged soot. Furthermore, the explorative TPR runs, performed by feeding reaction gases (NO and O_2) through fixed beds of any of the prepared catalyst in the absence of soot, led to just very little production of N_2 at least below 700 °C. This confirms that soot is actually needed as a reducing agent so as to enable the desired reduction of NO.

The main product of soot combustion was CO_2 of which the selectivity values always above 94% for any catalyst tested. Thus, CO_2 is generally the main product in soot oxidation. However, the investigations of $La_{1.7}Na_{0.3}CuO_4$ and $La_{1.3}Na_{0.7}CuO_4$ catalysts show that NO reduction occurred over a broader temperature interval. In the temperature range of 300–420 °C, the main product of NO reduction was N_2O. On the contrary, N_2 was the main product of NO reduction in the temperature range of 400–520 °C, and the selectivity towards N_2 production against N_2O was above 85%. Because the ranges of the main temperature peaks for soot combustion in all the samples were between 450 and 520 °C, it further demonstrated that soot combustion and NO reduction could take place simultaneously on the all perovskite-like catalysts.

Fig. 9 shows the outlet concentrations of CO_2 and NO over $La_{1.7}Na_{0.3}CuO_4$ and $La_{1.3}Na_{0.7}CuO_4$ catalysts at the various reactant gaseous compositions. In the absence of oxygen, CO_2 is produced at very high temperatures, which is due to the soot oxidation by lattice oxygen. In the presence of NO and oxygen, outlet CO_2 concentration early reached a maximum. Thus, T_{10} is dependent on the composition of reaction gases and it follows the order: NO > O_2 > NO + O_2. The lowest T_{10} in the NO + O_2 gas strongly suggests such a mechanism that the reaction is accelerated by the cooperation of nitric oxide and oxygen, e.g. the implication of nitrogen dioxide. NO_2 is much more reactive towards soot than NO as it was confirmed by literature [30,31]. Formation of NO_2 by NO oxidation is proven in Fig. 8. The TPR result shows that NO_2 was formed above 250 °C and its content decreased during soot combustion due to the reaction between NO_2 and soot. Therefore, nitrogen dioxide can directly accelerate the combustion rate of soot.

4.2. The correlation between the structures of catalysts and the catalytic performances for simultaneous removal of NO_x and diesel soot

The performances of catalyst materials depend on their structures. It is interesting to assess the role played by the A-site ions in perovskite-like oxides on this peculiar catalytic behavior. In the Ln_2CuO_4 catalysts, as shown in Table 5, the

Table 5
The catalytic performances of Ln_2CuO_4 and $La_{2-x}Na_xCuO_4$ catalysts for the simultaneous removal of soot and NO_x under loose contact conditions between the catalysts and soot (Ln = La, Pr, Nd, Sm, Gd, and x = 0, 0.1, 0.3, 0.5, 0.7, 0.9)

Catalysts	S_{CO_2}	T_{10}	T_{50}	T_{90}	P_{N_2}
La_2CuO_4	95.8	439.8	503.9	541.1	10.3
Pr_2CuO_4	96.9	440.8	506.8	543.9	10.5
Nd_2CuO_4	95.6	446.7	518.5	545.7	9.4
Sm_2CuO_4	95.6	449.5	518.4	547.5	9.2
Gd_2CuO_4	94.8	452.2	520.1	552.3	8.8
$La_{1.9}Na_{0.1}CuO_4$	96.2	438.8	502.9	538.7	11.4
$La_{1.7}Na_{0.3}CuO_4$	97.1	429	478.3	515	21.4
$La_{1.5}Na_{0.5}CuO_4$	97.4	408.1	470.1	519	13.8
$La_{1.3}Na_{0.7}CuO_4$	97.5	398.4	463.5	506.3	13.6
$La_{1.1}Na_{0.9}CuO_4$	97.2	406.3	464.5	510.6	13.1
La7-9	96.2	456.8	501.8	542.5	19.2
La3-9	96.3	454.2	500.4	541.8	13.4

change of the catalytic activity is very small for different rare earth atoms. It reveals that only changing the rare earth composition at A-site is difficult to promote the catalytic performance for the simultaneous removal of NO and soot. Whereas, the catalytic activity is strongly affected by the substitution of alkali metal ions into A-site. The introduction of Na in the lattice of the above perovskite-like at the nine-fold coordinated A-site (ionic radii: La^{3+} = 0.136 nm, Na^+ = 0.138 nm) leads to a significant decrease of T_{10} and remarkable increase of P_{N_2}. For perovskite-like oxide catalyst, the cation at A-site (La^{3+}) is generally trivalent, as La^{3+} at A-site is replaced by lower valency cation Na^+, according to the principle of electron neutrality, the positive charge reduced could be balanced either by the formation of higher oxidation state ion at B-site [32,33], i.e.,

$$Cu^{2+} \rightarrow Cu^{3+}$$

$$La_{2-x}Na_xCu^{2+}{}_{1-2x}Cu^{3+}{}_{2x}O_4 \rightarrow La_2CuO_4 + xLa^{3+}|Na^+|'' + 2xCu^{2+}|Cu^{3+}|$$

or by the formation of oxygen vacancy (V_o) in $La_{2-x}Na_xCuO_4$.

$$La_{2-x}Na_x\lambda(V_o)Cu^{2+}O_{4-\lambda} \rightarrow La_2CuO_4 + xLa^{3+}|Na^+|'' + \lambda|O|^{\bullet\bullet}$$

With increasing the values of x, the concentration of unstable Cu^{3+} and/or of oxygen vacancies also increase, which favors the diffusion of lattice oxygen from the bulk to surface, as charge compensators. Thus, the increasing of Na content in the defective structure of $La_{2-x}Na_xCuO_4$ accounts for the enhancing of the catalytic activity.

Based on the above discussion, the following three reasons can lead to the activity enhancement for Na-substituted samples compared to the unsubstituted sample (La_2CuO_4). The first one is that A-site cation (La^{3+}) is partly replaced by Na^+ and partial Cu^{2+} changed to Cu^{3+}, which had better catalytic oxidation activity than Cu^{2+}. Therefore, it can lower the temperature of soot combustion. The second one is the increase of the oxygen vacancy (V_o) content in $La_{2-x}Na_xCuO_4$. The presence of a large amount of oxygen vacancies would accelerate the mobility of

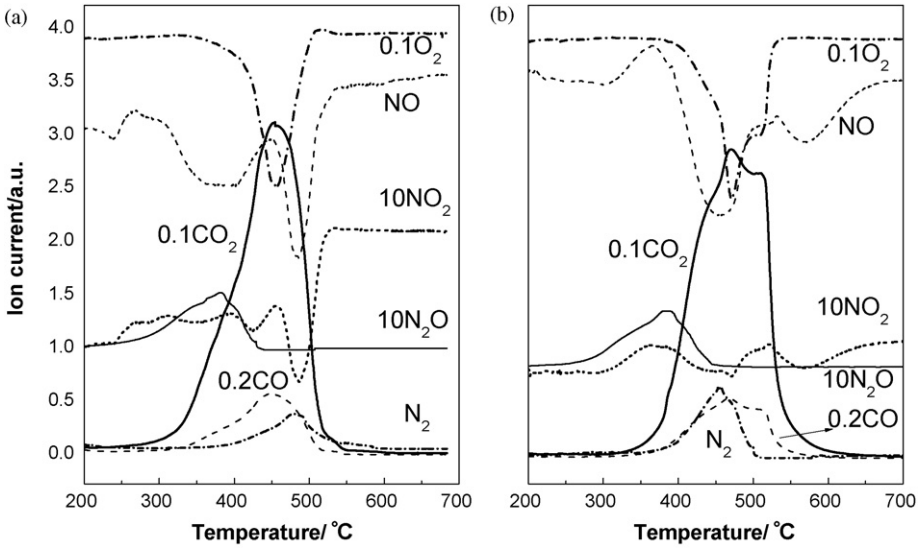

Fig. 8. The results of TPR over $La_{1.7}Na_{0.3}CuO_4$ and $La_{1.3}Na_{0.7}CuO_4$ catalysts under loose contact conditions between the catalysts and soot (a) $La_{1.3}Na_{0.7}CuO_4$ and (b) $La_{1.7}Na_{0.3}CuO_4$.

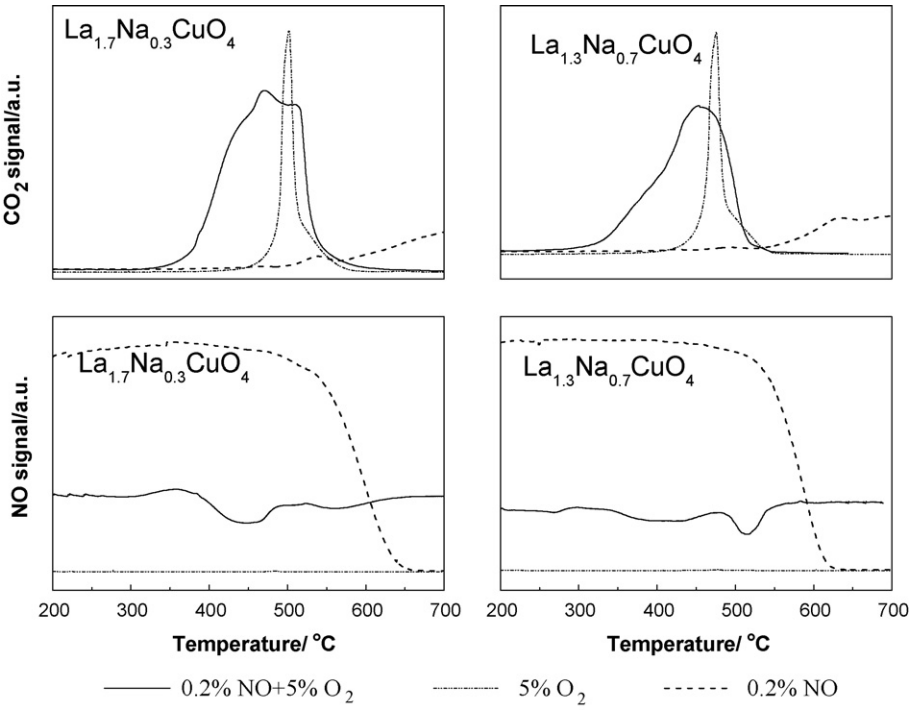

Fig. 9. The outlet CO_2 or NO concentration plots over $La_{1.7}Na_{0.3}CuO_4$ and $La_{1.3}Na_{0.7}CuO_4$ catalysts at the different reactant gas compositions under loose contact conditions between the catalysts and soot.

lattice oxygen and facilitate to the reproduction of oxygen vacancy, which increases the adsorption and activation of NO or molecular oxygen of catalyst surface. Therefore, it can improve the catalytic activity for simultaneous removal NO_x and soot. As shown in Tables 2 and 5, there was a good consistence between the nonstoichiometric oxygen content and the catalytic activity. Moreover, Fig. 4 exhibits that the peak area of H_2-TPR reduction increased with the increasing of Na substitution amount. It reveals that the mobility of oxygen increases in $La_{2-x}Na_xCuO_4$ catalysts, which enhances their catalytic activities for simultaneous removal NO_x and soot. Furthermore, Fig. 6 shows that the peak areas of NO-TPD increase with the Na substitution amount. This result indicates that the adsorption of NO is strongly related to the oxygen vacancy concentration. However, the catalytic activity toward NO_x reduction did not enhance in the range of $x \geq 0.5$ with the increasing of x. Fig. 7 and Table 5 show the catalytic activity for removal of NO was proportional to the amount of absorbed NO under the oxygen-rich conditions rather than under the oxygen-free conditions. This result indicates that the adsorption of NO is significant to the activation of NO molecule. The last one is that NO_2 was generated from the oxidation of the NO over these perovskite-like catalysts. NO_2 is a stronger oxidant than O_2 and NO_2 molecular is easy to contact with soot particulates, which can oxidize soot at a relatively low temperature. Thus, the oxidation temperature of soot becomes lower under loose contact conditions.

Finally, it is noteworthy that the catalytic activities of Ln-Na-Cu-O perovskite-like oxide catalysts prepared in this study are much higher than those of similar catalysts in the open literatures for soot combustion under loose contact conditions between soot and the catalyst [9]. The reason is that the sizes of Ln-Na-Cu-O perovskite-like oxides were in the nanometer range. The surface particle sizes of nanometric catalyst are small and their surface atoms have extra and high surface energy. Thus, the surface atoms are good at mobility. Combined the both roles of nanoparticle effect and NO_2 formation, the contact is still very good between catalyst and soot even under loose contact conditions.

5. Conclusions

(1) The nanometric Ln-Na-Cu-O perovskite-like complex oxide catalysts can be obtained by sol–gel auto-combustion method. Under loose contact conditions between soot and the catalyst, the nanometric Ln-Na-Cu-O perovskite-like oxides have good catalytic activities for the simultaneous removal of diesel soot and NO_x.

(2) In the Ln_2CuO_4 catalysts, with the increase of atomic number the catalytic activity became gradually lower. However, in the $La_{2-x}Na_xCuO_4$ catalysts the partial substitution of Na for La at A-site remarkably enhanced their catalytic activities attributing to the formations of Cu^{3+} and nonstoichiometry oxygen (λ). The oxygen vacancy has an important effect on the catalytic activity because the oxygen vacancy is beneficial to enhance the adsorption and activation of NO or molecular oxygen. The change of λ value is consistent with that of the catalytic activity for soot combustion with the increase of x value.

(3) NO_2 can be generated from the NO catalytic oxidation over these perovskite-like catalysts. It also accelerated the soot

combustion rate due to the strong oxidation ability of NO_2 and the good mobility of NO_2 molecule, and thus the good contact property of NO_2 and soot particles.

(4) It was found that complex oxides with perovskite-like structure possess different adsorption behaviors under the conditions with or without oxygen. The catalytic performances of these catalysts for NO removal are closely related to their NO adsorption characters under the oxygen-rich condition.

Acknowledgements

This work was supported by the National Natural Science Foundation of China (Nos. 20473053 and 20525021), the Beijing Natural Science Foundation in China (No. 2062020), the 863 program of China (No. 2006AA06Z346), and the Scientific Research Key Foundation for the Returned Overseas Chinese Scholars of State Education Ministry.

References

[1] Z.P. Liu, S.J. Jenkins, D.A. King, J. Am. Chem. Soc. 126 (2004) 10746.
[2] J. Liu, Z. Zhao, C.M. Xu, A.J. Duan, L. Zhu, X.Z. Wang, Appl. Catal. B 61 (2005) 39.
[3] S. Kureti, W. Weisweiler, K. Hizbullah, Appl. Catal. B 43 (2003) 281.
[4] K. Yoshida, S. Makino, S. Sumiya, G. Muramatsu, R. Helferich, SAE Paper, 892046, 1989.
[5] Y. Teraoka, K. Nakano, S. Kagawa, W.F. Shangguan, Appl. Catal. B 5 (1995) L181.
[6] Y. Teraoka, K. Nakano, W.F. Shangguan, S. Kagawa, Catal. Today 27 (1996) 107.
[7] W.F. Shangguan, Y. Teraoka, S. Kagawa, Appl. Catal. B 16 (1998) 149.
[8] S.S. Hong, G.D. Lee, Catal. Today 63 (2000) 397.
[9] D. Fino, P. Fino, G. Saracco, V. Specchia, Appl. Catal. B 43 (2003) 243.
[10] T. Miyazaki, N. Tokabuchi, M. Arita, M. Inoue, I. Mochida, Energy Fuel 11 (1997) 832.
[11] Y. Teraoka, K. Kanada, S. Kagawa, Appl. Catal. B 34 (2001) 73.
[12] W.F. Shangguan, Y. Teraoka, S. Kagawa, Appl. Catal. B 8 (1996) 217.
[13] J.P.A. Neeft, M. Michiel, A. Jacob, Appl. Catal. B 8 (1996) 57.
[14] Z. Zhao, A. Obuchi, J. Oi-Uchisawa, A. Ogata, S. Kushiyama, Chem. Lett. 4 (1998) 367.
[15] J. Oi-Uchisawa, A. Obuchi, S.D. Wang, T. Nanba, A. Ohi, Appl. Catal. B 43 (2003) 117.
[16] J. Oi-Uchisawa, S.D. Wang, T. Nanba, A. Ohi, A. Obuchi, Appl. Catal. B 44 (2003) 207.
[17] X.G. Peng, L. Manna, W.D. Yang, J. Wickham, E. Scher, A. Kadavanich, A.P. Alivisatas, Nature 404 (2000) 59.
[18] J.A. Schwarz, C. Contescu, A. Contescu, Chem. Rev. 95 (1995) 477.
[19] M. Li, H. Schnablegger, S. Mann, Nature 402 (1999) 393.
[20] D.C. Harris, T.A. Hewston, J. Solid State Chem. 69 (1987) 182.
[21] J. Liu, Z. Zhao, C.M. Xu, A.J. Duan, T. Meng, X.J. Bao, Catal. Today 119 (2007) 267.
[22] C.B. Liu, Z. Zhao, X.K. Ye, Y. Wu, Sci. China 40 (1997) 513.
[23] N. Ogita, M. Udagawa, K. Kojima, J. Phys. Soc. Jpn. 57 (1989) 3982.
[24] W.J.J. Potts, Chem. Infrared Spectroscopy, vol. 1, John Wiley, New York, London, Sydney, 1963, p. 135.
[25] Z. Zhao, Y. Yamada, A. Ueda, H. Sakurai, T. Kobayashi, Catal. Today 93–95 (2004) 163.
[26] R. Spinicci, A. Tofanari, Catal. Today 8 (1990) 473.
[27] P.A.J. Neeft, M. Makkee, J.A. Moulijn, Appl. Catal. B 8 (1996) 57.
[28] A. Carrascull, I.D. Lick, N.P. Esther, M.I. Ponzi, Catal. Commun. 4 (2003) 124.
[29] J.V. Craenenbroeck, D. Andreeva, T. Tabakova, K.V. Werde, J. Mullens, F. Verpoort, J. Catal. 209 (2002) 515.
[30] S. Liu, A. Obuchi, J. Oi-Uchisawa, T. Nanba, S. Kushiyama, Appl. Catal. B 37 (2002) 309.
[31] J. Oi-Uchisawa, A. Obuchi, R. Enomoto, J. Xu, T. Nanba, S. Liu, S. Kushiyama, Appl. Catal. B 32 (2001) 257.
[32] Y. Wu, Z. Zhao, Y. Liu, X.G. Yang, J. Mol. Catal. A 155 (2000) 89.
[33] H. Falcon, M.J. Martinez-Lope, J.A. Alonso, J.L.G. Fierro, Appl. Catal. B 26 (2003) 131.